Journal of Solid Mechanics Vol. 15, No. 2 (2023) pp. 225-243
DOI: 10.22034/jsm.2022.1962151.1747

Research Paper

Fracture Analysis of Several Interface Cracks in an FG Half-Plane with a Homogeneous Coating under Mixed-Mode Transient Loading

R. Bagheri [1,*], M. Ayatollahi [2], S.M. Hosseini [1], A. Bagheri [3]

[1] *Department of Mechanical Engineering, Karaj Branch, Islamic Azad University, Karaj, Iran*
[2] *Faculty of Engineering, University of Zanjan, Zanjan, Iran*
[3] *Department of Mathematics, Payame Noor University, Ardabil, Iran*

Received 28 March 2023; accepted 18 May 2023

ABSTRACT

In this paper, the mechanical fracture problem of a half-plane made of functionally graded material (FGM) with a coating of a homogeneous layer containing multiple interface cracks is investigated in order to determine the dynamic stress intensity factors (DSIFs) under transient in-plane loading. According to exponential law, the properties of functionally graded material change continuously along *y*-direction. Initially, integral transformations and dislocation of the Volterra type of climbing and sliding edges on the interface of a FG half-plane with a homogeneous coating leads to the numerical solution of a system with singular integral equations. These equations which have the Cauchy type-singularity are then obtained using the distributed dislocation technique (DDT). Using the inversion technique in the Laplace domain, the dislocation density on the crack faces is obtained which has led to the determination of the DSIFs. Finally, in order to show the accuracy and validity of this research, the final results in the form of graphs have been compared with other references and a very acceptable conformity has been observed. The influences of the FG parameter, coating thickness, crack length, the variation of time and the interaction between of cracks on the DSIFs are studied.

Keywords: Several interface cracks; FGM half-plane; In-plane loading; Homogeneous coating; Dislocation method.

1 INTRODUCTION

IN recent years, FGMs which represent a new version of composite materials with continuous variation of the elastic and physical properties, have become the research interest of many scientists due to their high performance optimization, improved mechanical properties, and thermal corrosion resistance. To solve the differential equations governing the medium made of FGMs, variable coefficients must be used instead of constants. From the behavioral perspective of failure mechanics, due to the complexity of crack growth analysis of FGM materials, the study of

*Corresponding author.
*E-mail address: r.bagheri@kiau.ac.ir (*R.Bagheri)

DSIFs for use in more reliable designing involving FGMs can be a significant field of scientific research. In studies conducted by researchers, it has been shown that for interface cracks, the properties of materials especially FGMs play an considerable role in their mechanical fracture behavior. The various problems of fracture mechanics in FGMs are solved under in-plane loading. A brief review of the articles on cracks under the in-plane load is listed below. Ma et al. [1] studied the dynamic behavior of two collinear cracks in FGM layer bonded to dissimilar half planes under anti-plane shear waves by the Schmidt method. The effects of the geometry of the interacting cracks, the shear stress wave velocity of the materials and the frequency of the incident wave on the DSIFs are investigated. The crack problem for a partially insulated interface crack between a functionally graded coating and a homogeneous substrate subject to both thermal and mechanical loading was considered by El-Borgi et al [2]. The problem is solved under the assumption of plane strain and generalized plane stress conditions. Chi and Chung [3] studied the SIF of cracked multi-layered and FGM coatings of a coating–substrate composite, due to the action of uniform normal stress on the crack surfaces. In this paper, the substrate is assumed to be homogeneous material, while the coating consists of multi-layered media or sigmoid FGMs. A new multi-layered model for fracture analysis of FGMs with arbitrarily varying elastic moduli under plane deformation was investigated by Huang et al. [4]. In this investigation, the FGM is divided into several sub-layers and in each sub-layer the shear modulus is assumed to be a linear function of the depth while the Poisson's ratio is assumed to be a constant. The DSIFs around two parallel cracks in a functionally graded layer bonded to dissimilar half-planes under an anti-plane incident harmonic loading is studied by Ma et al. [5]. The Fourier transform technique is used to reduce the boundary conditions to four simultaneous integral equations which are then solved by expanding the differences of crack surface displacements in a series. An interface crack problems in graded orthotropic media using analytical and computational techniques was investigated by Dag et al. [6]. Mechanical properties of the medium are assumed to be continuous with discontinuous derivatives at the interface. Liu et al. [7] provided a method for obtaining the mixed-mode stress intensity factors for a bi-material interface crack in the infinite strip configuration and in the case where both phases are fully anisotropic. Guo et al. [8] studied the transient response of a coating–substrate structure with a cracked functionally graded interfacial layer subjected to an impact load. In this study, the influences of the material nonhomogeneity constant and the geometry parameters on the DSIFs are investigated. Li [9] analyzed the problem of an interface crack between two bonded dissimilar semi-infinitely long orthotropic strips of finite width under arbitrary anti-plane shear loading. The finite Fourier transform technique is used to reduce the mixed boundary value problem to triple series equations, which are then transformed to a singular integral equation. A new multi-layered model for fracture analysis of functionally graded materials (FGMs) with arbitrarily varying Young's modulus and Poisson's ratio under plane stress-state deformation is developed by Huang et al. [10]. Chen [11] investigated thermal fracture problem of an interface crack between a graded orthotropic coating and the homogeneous substrate by two different approaches. In this paper, the influence of material gradient parameters and material distribution on the thermal fracture behavior is presented. The plane elasticity problem of an arbitrarily oriented crack in an FGM layer bonded to a homogeneous half-plane was studied by Long and Delale [12]. They analyzed the effects of the crack length, crack orientation and the non-homogeneity parameter of the strip material on the fracture of the FGM layer. Yong dong et al. [13] established the mechanical model for the dynamic fracture problem of the weak-discontinuous interface between an FGM coating and an FGM substrate. The Cauchy singular integral equation for the crack is derived by integral transform, and the allocation method is used to get the numerical solution. Ioka et al. [14] calculated the stress distributions on the interface of bonded dissimilar materials with an interlayer by using the boundary element method to investigate the effect of the interlayer on the stress distribution. The relation between the free-edge singular stress fields of bonded dissimilar materials with and without an interlayer was investigated numerically. Li and Fan [15] analyzed the transient response of a crack embedded in a functionally graded material (FGM) layer sandwiched between two dissimilar elastic layers under anti-plane shear impact loads. The material properties of the FGM are assumed to be an exponential function of the thickness. Guo and Noda [16] analyzed the dynamic response of a functionally graded layered structure with a crack crossing the interface. By using the Laplace and Fourier integral transforms, singular integral equation method and residue theory, the present problem is reduced to a singular integral equation in the Laplace transform domain. Li and Lee [17] extended the concept of weak discontinuity to the interface in FGPMs, and investigated the fracture behavior of a weak discontinuous interface between two piezoelectric strips under electromechanical loads by the methods of Fourier integral transform and Cauchy singular integral equation. The dynamic response of a magnetoelectroelastic half-space with a functionally graded coating containing crack at the interface when subjected to sudden impacts is studied by Peng and Li [18]. In this paper, by using the integral transform method, the problem is reduced to solving singular integral equations. Torshizian and Kargarnovin [19] is considered an internal crack located within a functionally graded material (FGM) strip bonded with two dissimilar half-planes and under an anti-plane load. The crack is oriented in an arbitrary direction and the material properties of the strip are assumed to vary exponentially in the thickness

direction and two half-planes are assumed to be isotropic. Cheng et al. [20] is studied a finite crack with constant length propagating in a functionally graded coating with spatially varying elastic properties bonded to a homogeneous substrate finite thickness under anti-plane loading. A multi-layered model is employed to model arbitrary variations of material properties based on two linearly-distributed material compliance parameters. In another work, Cheng et al. [21] analyzed the problem of a finite interface crack with constant length propagating along the interface between two dissimilar functionally graded strips with spatially varying elastic properties under in-plane loading. By utilizing the Fourier transform technique, the mixed boundary problem is reduced to a system of singular integral equations that are solved numerically. Shi [22] investigated the problem of a doubly periodic interface crack in a layered periodic composite under anti-plane shear loads. In this study, the shielding effect of multiple parallel cracks and the amplifying effect of multiple collinear cracks exist simultaneously, and a coupled effect between geometrical and physical parameters on the interfacial fracture behavior exists clearly. In recent years, by utilizing the distributed dislocation technique (DDT), more complicated problems including several cracks with any arrangement have been solved. A concise review of articles is presented here. The analytical solution of two functionally graded layers with Volterra type screw dislocation anti-plane shear impact loading were investigated by Fallahnejad et al. [23]. The energy dissipation of FGM layers is modeled by viscous damping and the properties of the materials are assumed to change exponentially along the thickness of the layers. Bagheri [24] studied the analytical solution of two dissimilar orthotropic functionally graded half-layers with interface Volterra-type screw dislocation under anti-plane transient loading using linear elasticity theory. The dynamic stress intensity factors (DSIFs) are calculated in time domain by using numerical Laplace inversion and the distributed dislocation technique. The mixed mode analysis of multiple cracks in two dissimilar half-planes under transient loading, steady-state condition and time-harmonic loading were calculated by Bagheri and Monfared [25-26] and Bagheri and Enjilela [27], respectively. In these papers, in-plane loading is considered and it is assumed that the properties of the non-homogeneous material change exponentially. Mode III DSIFs of several axisymmetric interfacial cracks in an FGM coated orthotropic layer, transient analysis for torsional impact of multiple axisymmetric cracks in the FG orthotropic medium and computation of mixed mode SIFs for multiple axisymmetric cracks in an FGM medium under transient loading were analyzed by Bagherpoor and Pourseifi [28], Rabieifar et al. [29] and Monfared et al. [30], respectively.In accordance with the review of the above literature, there is no favorable investigation for the transient response of multiple cracks at the interface of an FG half-plane with homogeneous coating under mixed mode loading.

In this paper, the problem of multiple cracks located between an FG half-plane substrate and a homogeneous coating under mixed-mode loads is investigated using DDT. First, using the dislocation solution and integral transforms in conjunction with the Lobatto–Chebyshev collocation and the Stehfest's method [31], the singular integral equations with Cauchy singularity form are extracted and are solved numerically for the dislocation density on the cracks faces. Then, these solutions are used to calculate mixed-mode DSIFs for multiple interface cracks. Consideration will be concentrated on the effects of the time variations, coating thickness, the gradient of the material property and as well as crack interactions on transient SIFs.

2 DISLOCATION SOLUTIONS

Assuming perfect bonding between the two mediums, to reinforce the FGM half-plane, a layer of homogeneous coating with thickness h is used as shown in Fig. 1 that contain a Volterra dislocation in the positive direction of x-axis. The x and y indicate the Cartesian coordinate system which defines x-axis to the right along the interface and the y-axis facing upwards in the coating thickness direction.

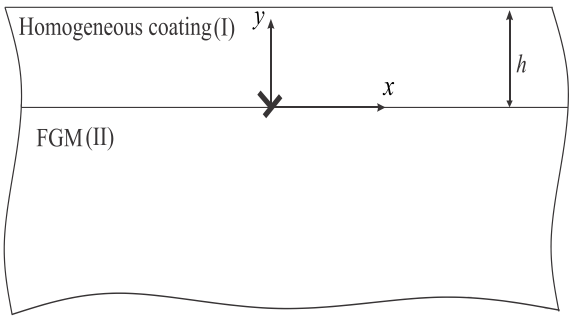

Fig.1
Schematic of a dislocation at the interface between the coating and the substrate.

In this case, since our assumption is based on the propagation of cracks in a plane, therefore the constitutive equations in terms of elastic displacements in the half-plane FGM in the absence of body force will be written as follows:

$$\begin{aligned}
&\sigma_{xx}(x,y,t)=\frac{\mu_0 e^{\beta y}}{\kappa-1}[(\kappa+1)u_{,x}+(3-\kappa)v_{,y}]\\
&\sigma_{yy}(x,y,t)=\frac{\mu_0 e^{\beta y}}{\kappa-1}[(3-\kappa)u_{,x}+(\kappa+1)v_{,y}]\\
&\tau_{xy}(x,y,t)=\mu_0 e^{\beta y}(u_{,y}+v_{,x}) \quad y\le 0
\end{aligned} \tag{1}$$

where u , v are the in-plane displacements in the x and y direction, respectively, $\sigma_{xx},\sigma_{yy},\tau_{xy}$ are the stress tensor components, μ_0 and κ denotes the shear modulus of elasticity at *th* interface and the Kolosov constant, respectively. The Kolosov constant is $\kappa=(3-\upsilon)/(1+\upsilon)$ for plane stress and $\kappa=3-4\upsilon$ for plane strain, where indicates the Poisson ratio of the material. In addition, in the above relations, comma denotes partial derivatives. By placing Eqs. (1) in the equations of motion, $\sigma_{ij,j}=\rho(y)u_{i,tt},(i,j)\in\{x,y\}$, these equations for the FGM half-plane are easily written in terms of displacements as follows:

$$\begin{aligned}
&(\kappa+1)u_{,xx}+2v_{,xy}+(\kappa-1)u_{,yy}+\beta(\kappa-1)(u_{,y}+v_{,x})=c^2(\kappa-1)u_{,tt}\\
&(\kappa-1)v_{,xx}+2u_{,xy}+(\kappa+1)v_{,yy}+\beta(\kappa+1)v_{,y}+\beta(3-\kappa)u_{,x}=c^2(\kappa-1)v_{,tt} \qquad y\le 0
\end{aligned} \tag{2}$$

Based on an accepted logical presumption and in order to simplify the solution of the governing differential equations, the focus will be on a specific type of FGMs in which the constants of nonhomogeneous material change according to the exponential laws as follows:

$$\rho(y)=\rho_0 e^{\beta y} \tag{3}$$

where ρ_0 and μ_0 refers to the material density in the $y=0$ location and elastic constant at interface and β is a constant that indicates the distribution of non-homogeneous materials. By placing $\beta=0$ in relations (2), the equations of motion for homogeneous coating $0\le y\le h$ are acquired as follows:

$$\begin{aligned}
&(\kappa+1)u_{,xx}+2v_{,xy}+(\kappa-1)u_{,yy}=c^2(\kappa-1)u_{,tt}\\
&(\kappa-1)v_{,xx}+2u_{,xy}+(\kappa+1)v_{,yy}=c^2(\kappa-1)v_{,tt} \qquad 0\le y\le h
\end{aligned} \tag{4}$$

where $1/c=\sqrt{\mu_0/\rho_0}$ demonstrate the shear wave velocity at the interface of two materials. As shown in Fig.1, let a Volterra glide and climb of the edge dislocations with Burgers vectors $b_x(t)$ and $b_y(t)$ be situated at the origin of the coordinates with the dislocation line $y=0, x>0$. According to the displacement jumps defined by the Volterra edge dislocations, the conditions of displacement and continuous stress as well as the traction free conditions on the boundaries governing the problem can be expressed as follows:

$$\begin{aligned}
&u(x,0^+,t)-u(x,0^-,t)=b_x(t)H(x) \quad , v(x,0^+,t)-v(x,0^-,t)=b_y(t)H(x)\\
&\sigma_{yy}(x,0^+,t)=\sigma_{yy}(x,0^-,t) \quad , \quad \tau_{xy}(x,0^+,t)=\tau_{xy}(x,0^-,t)\\
&\sigma_{yy}(x,h,t)=0 \quad , \ \tau_{xy}(x,h,t)=0\\
&\lim_{y\to-\infty}\sigma_{ij}=0, \quad (i,j)\in\{x,y\} \quad , \ \lim_{y\to-\infty}u=\lim_{y\to-\infty}v=0
\end{aligned} \tag{5}$$

where $H(.)$ is the Heaviside step function. It is supposed that the study medium is at rest at time; hence, by applying

Laplace and Fourier transform to Eqs. (2) and (4) to the variables t and x, respectively, and assuming that the stress components in the far field are zero, the following results are obtained:

$$\begin{cases}(\kappa-1)U^*_{,yy}+\beta(\kappa-1)U^*_{,y}+2i\zeta V^*_{,y}+i\zeta\beta(\kappa-1)V^*-[\zeta^2(\kappa+1)+c^2(\kappa-1)s^2]U^*=0\\(\kappa+1)V^*_{,yy}+\beta(\kappa+1)V^*_{,y}+2i\zeta U^*_{,y}+i\zeta\beta(3-\kappa)U^*-[\zeta^2(\kappa-1)+c^2(\kappa-1)s^2]V^*=0\end{cases}\quad y\le 0 \tag{6a}$$

$$\begin{cases}(\kappa-1)U^*_{,yy}+2i\zeta V^*_{,y}-[\zeta^2(\kappa+1)+c^2(\kappa-1)s^2]U^*=0\\(\kappa+1)V^*_{,yy}+2i\zeta U^*_{,y}-[\zeta^2(\kappa-1)+c^2(\kappa-1)s^2]V^*=0\end{cases}\quad 0\le y\le h \tag{6b}$$

where the superscript $*$ represents the Laplace transform, the s is Laplace variable at the time transform domain, $i=\sqrt{-1}$, ζ is the Fourier variable, and U and V are Fourier transforms of displacement components u and v, respectively. By solving the differential Eqs. (6a) and (6b) for both regions $y\le 0$, and $0\le y\le h$, the following results are obtained for U^* and V^*:

$$\begin{cases}U^*(\zeta,y,s)=A_1e^{\lambda_1 y}+A_2e^{\lambda_2 y}+A_3e^{\lambda_3 y}+A_4e^{\lambda_4 y}\\V^*(\zeta,y,s)=ia_{11}A_1e^{\lambda_1 y}+ia_{21}A_2e^{\lambda_2 y}+ia_{31}A_3e^{\lambda_3 y}+ia_{41}A_4e^{\lambda_4 y}\end{cases}\quad y\le 0 \tag{7a}$$

$$\begin{cases}U^*(\zeta,y,s)=C_1e^{r_1 y}+C_2e^{r_2 y}+C_3e^{r_3 y}+C_4e^{r_4 y}\\V^*(\zeta,y,s)=ib_{11}C_1e^{r_1 y}+ib_{21}C_2e^{r_2 y}+ib_{31}C_3e^{r_3 y}+ib_{41}C_4e^{r_4 y}\end{cases}\quad 0\le y\le h \tag{7b}$$

where $\{A_j,C_j\},j=1,2,3,4$ are the unknown functions. The characteristic roots $\{\lambda_j,r_j\},j=1,2,3,4$ and the functions $\{a_{j1},b_{j1}\},j=1,2,3,4$ are given as:

$$\begin{cases}\lambda_1=\frac{1}{2}[-\beta-\sqrt{\beta^2-2\Delta_3+2\sqrt{\Delta_3^2-4\Delta_4}}],\lambda_2=\frac{1}{2}[-\beta-\sqrt{\beta^2-2\Delta_3-2\sqrt{\Delta_3^2-4\Delta_4}}],\quad \mathrm{Re}(\lambda_1,\lambda_2)<0\\\lambda_3=\frac{1}{2}[-\beta+\sqrt{\beta^2-2\Delta_3+2\sqrt{\Delta_3^2-4\Delta_4}}],\lambda_4=\frac{1}{2}[-\beta+\sqrt{\beta^2-2\Delta_3-2\sqrt{\Delta_3^2-4\Delta_4}}],\quad \mathrm{Re}(\lambda_3,\lambda_4)>0\quad y\le 0\\a_{j1}=\dfrac{(\kappa-1)\lambda_j^2+\beta(\kappa-1)\lambda_j-[\zeta^2(\kappa+1)+c^2(\kappa-1)s^2]}{\zeta[2\lambda_j+\beta(\kappa-1)]},\ j=1,2,3,4\end{cases} \tag{8a}$$

$$\begin{cases}r_1=\sqrt{\zeta^2+c^2s^2},r_2=\sqrt{\zeta^2+c^2s^2\dfrac{\kappa-1}{\kappa+1}},\quad \mathrm{Re}(r_1,r_2)>0\\r_3=-\sqrt{\zeta^2+c^2s^2},r_4=-\sqrt{\zeta^2+c^2s^2\dfrac{\kappa-1}{\kappa+1}},\quad \mathrm{Re}(r_3,r_4)<0\qquad 0\le y\le h\\b_{j1}=\dfrac{(\kappa-1)r_j^2-[\zeta^2(\kappa+1)+c^2(\kappa-1)s^2]}{2\zeta r_j},\ j=1,2,3,4\end{cases} \tag{8b}$$

where

$$\begin{aligned}\Delta_3&=-2\zeta^2-\frac{2c^2\kappa s^2}{\kappa+1}\\\Delta_4&=\zeta^4+\frac{2c^2\kappa s^2\zeta^2}{\kappa+1}+\frac{c^4s^4(\kappa-1)}{\kappa+1}-\zeta^2\beta^2\frac{\kappa-3}{\kappa+1}\end{aligned} \tag{9}$$

Since the displacements in Eqs. (7a) should be limited at $y=-\infty$, the unknown functions A_1, A_2 become zero. By taking the inverse Fourier transform, the displacement fields in Eqs. (7a) and (7b) lead to the following results:

$$\begin{cases} u^*(x,y,s)=\dfrac{1}{2\pi}\displaystyle\int_{-\infty}^{\infty}(A_3e^{\lambda_3 y}+A_4e^{\lambda_4 y})e^{i\zeta x}d\zeta \\ v^*(x,y,s)=\dfrac{i}{2\pi}\displaystyle\int_{-\infty}^{\infty}(a_{31}A_3e^{\lambda_3 y}+a_{41}A_4e^{\lambda_4 y})e^{i\zeta x}d\zeta \end{cases} \qquad y\le 0 \tag{10a}$$

$$\begin{cases} u^*(x,y,s)=\dfrac{1}{2\pi}\displaystyle\int_{-\infty}^{\infty}(C_1e^{r_1 y}+C_2e^{r_2 y}+C_3e^{r_3 y}+C_4e^{r_4 y})e^{i\zeta x}d\zeta \\ v^*(x,y,s)=\dfrac{i}{2\pi}\displaystyle\int_{-\infty}^{\infty}(b_{11}C_1e^{r_1 y}+b_{21}C_2e^{r_2 y}+b_{31}C_3e^{r_3 y}+b_{41}C_4e^{r_4 y})e^{i\zeta x}d\zeta \end{cases} \qquad 0\le y\le h \tag{10b}$$

Finally, using the Eqs. (1), (10a) and (10b), the stress components in the Laplace domain for the two regions under study can be expressed as follows:

$$\begin{cases} \sigma_{xx}^*(x,y,s)=\dfrac{i\mu_0e^{\beta y}}{2\pi(\kappa-1)}\displaystyle\int_{-\infty}^{\infty}(a_{32}A_3e^{\lambda_3 y}+a_{42}A_4e^{\lambda_4 y})e^{i\zeta x}d\zeta \\ \sigma_{yy}^*(x,y,s)=\dfrac{i\mu_0e^{\beta y}}{2\pi(\kappa-1)}\displaystyle\int_{-\infty}^{\infty}(a_{33}A_3e^{\lambda_3 y}+a_{43}A_4e^{\lambda_4 y})e^{i\zeta x}d\zeta \\ \tau_{xy}^*(x,y,s)=\dfrac{\mu_0e^{\beta y}}{2\pi}\displaystyle\int_{-\infty}^{\infty}(a_{34}A_3e^{\lambda_3 y}+a_{44}A_4e^{\lambda_4 y})e^{i\zeta x}d\zeta \end{cases} \qquad y\le 0 \tag{11a}$$

$$\begin{cases} \sigma_{xx}^*(x,y,s)=\dfrac{i\mu_0}{2\pi(\kappa-1)}\displaystyle\int_{-\infty}^{\infty}(b_{12}C_1e^{r_1 y}+b_{22}C_2e^{r_2 y}+b_{32}C_3e^{r_3 y}+b_{42}C_4e^{r_4 y})e^{i\zeta x}d\zeta \\ \sigma_{yy}^*(x,y,s)=\dfrac{i\mu_0}{2\pi(\kappa-1)}\displaystyle\int_{-\infty}^{\infty}(b_{13}C_1e^{r_1 y}+b_{23}C_2e^{r_2 y}+b_{33}C_3e^{r_3 y}+b_{43}C_4e^{r_4 y})e^{i\zeta x}d\zeta \\ \tau_{xy}^*(x,y,s)=\dfrac{\mu_0}{2\pi}\displaystyle\int_{-\infty}^{\infty}(b_{14}C_1e^{r_1 y}+b_{24}C_2e^{r_2 y}+b_{34}C_3e^{r_3 y}+b_{44}C_4e^{r_4 y})e^{i\zeta x}d\zeta \end{cases} \qquad 0\le y\le h \tag{11b}$$

where, the functions $\{a_{j2},a_{j3},a_{j4}\}$, $j=3,4$ and $\{b_{j2},b_{j3},b_{j4}\}$, $j=1,2,3,4$ are given as:

$$\begin{cases} a_{j2}=(\kappa+1)\zeta+(3-\kappa)a_{j1}\lambda_j \\ a_{j3}=(3-\kappa)\zeta+(\kappa+1)a_{j1}\lambda_j \\ a_{j4}=\lambda_j-\zeta a_{j1} \end{cases} \qquad j=3,4$$

$$\begin{cases} b_{j2}=(\kappa+1)\zeta+(3-\kappa)b_{j1}r_j \\ b_{j3}=(3-\kappa)\zeta+(\kappa+1)b_{j1}r_j \\ b_{j4}=r_j-\zeta b_{j1} \end{cases} \qquad j=1,2,3,4 \tag{12}$$

By applying the Fourier and Laplace transforms to the boundary conditions (5) and by using the expressions obtained in Eqs. (7a-7b) and (11a-11b), the unknown coefficients ($A_j, j=3,4$ and $C_j, j=1,2,3,4$) can be obtained as follows:

$$A_j = [A_{j1} b_x(s) + i A_{j2} b_y(s)](\pi\delta(\zeta) - i/\zeta), \quad j=3,4 \tag{13a}$$

$$C_j = [C_{j1} b_x(s) + i C_{j2} b_y(s)](\pi\delta(\zeta) - i/\zeta), \quad j=1,2,3,4 \tag{13b}$$

where $\delta(.)$ is the Dirac delta function and $A_{j1}, A_{j2}, j \in \{3,4\}$ are given in Appendix I. Substituting Eq. (13a) into Eqs. (11a), the stress components in the half-plane made of FGM is obtained as follows:

$$\begin{cases} \sigma_{xx}^*(x,y,s) = \dfrac{\mu_0 e^{\beta y}}{2\pi(\kappa-1)} \displaystyle\int_{-\infty}^{\infty} \frac{e^{i\zeta x}}{\zeta} [(a_{32}A_{31}e^{\lambda_3 y} + a_{42}A_{41}e^{\lambda_4 y}) b_x(s) + i(a_{32}A_{32}e^{\lambda_3 y} + a_{42}A_{42}e^{\lambda_4 y}) b_y(s)] d\zeta \\ \sigma_{yy}^*(x,y,s) = \dfrac{\mu_0 e^{\beta y}}{2\pi(\kappa-1)} \displaystyle\int_{-\infty}^{\infty} \frac{e^{i\zeta x}}{\zeta} [(a_{33}A_{31}e^{\lambda_3 y} + a_{43}A_{41}e^{\lambda_4 y}) b_x(s) + i(a_{33}A_{32}e^{\lambda_3 y} + a_{43}A_{42}e^{\lambda_4 y}) b_y(s)] d\zeta \quad y \le 0 \\ \tau_{xy}^*(x,y,s) = \dfrac{-i\,\mu_0 e^{\beta y}}{2\pi} \displaystyle\int_{-\infty}^{\infty} \frac{e^{i\zeta x}}{\zeta} [(a_{34}A_{31}e^{\lambda_3 y} + a_{44}A_{41}e^{\lambda_4 y}) b_x(s) + i(a_{34}A_{32}e^{\lambda_3 y} + a_{44}A_{42}e^{\lambda_4 y}) b_y(s)] d\zeta \end{cases} \tag{14}$$

To perform a numerical calculation of the components of stress fields, the integrals mentioned in Eqs. (14) can be divided into odd and even parts and rewritten in the following equation form:

$$\begin{aligned} \sigma_{xx}^*(x,y,s) &= \int_0^{\infty} f_{xx}(x,y,s,\zeta) d\zeta, \\ \sigma_{yy}^*(x,y,s) &= \int_0^{\infty} f_{yy}(x,y,s,\zeta) d\zeta, \\ \tau_{xy}^*(x,y,s) &= \int_0^{\infty} f_{xy}(x,y,s,\zeta) d\zeta \end{aligned} \tag{15}$$

where $f_{xy}(x,y,s,\zeta), i,j \in \{x,y\}$ are defined as follows:

$$\begin{aligned} f_{xx}(x,y,s,\xi) &= \frac{\mu_0 e^{\beta y}}{\pi(\kappa-1)\xi} [(a_{32}A_{31}e^{\lambda_3 y} + a_{42}A_{41}e^{\lambda_4 y}) b_x(s)\cos(\xi x) - (a_{32}A_{32}e^{\lambda_3 y} + a_{42}A_{42}e^{\lambda_4 y}) b_y(s)\sin(\xi x)] \\ f_{yy}(x,y,s,\xi) &= \frac{\mu_0 e^{\beta y}}{\pi(\kappa-1)\xi} [(a_{33}A_{31}e^{\lambda_3 y} + a_{43}A_{41}e^{\lambda_4 y}) b_x(s)\cos(\xi x) - (a_{33}A_{32}e^{\lambda_3 y} + a_{43}A_{42}e^{\lambda_4 y}) b_y(s)\sin(\xi x)] \\ f_{xy}(x,y,s,\xi) &= \frac{\mu_0 e^{\beta y}}{\pi\xi} [(a_{34}A_{31}e^{\lambda_3 y} + a_{44}A_{41}e^{\lambda_4 y}) b_x(s)\sin(\xi x) + (a_{34}A_{32}e^{\lambda_3 y} + a_{44}A_{42}e^{\lambda_4 y}) b_y(s)\cos(\xi x)] \end{aligned} \tag{16}$$

Since the integrals of Eqs. (15) are infinite for adjacent points of dislocation, the singular behaviors of the kernels f_{ij} are investigated by asymptotic values of f_{ij} for $\zeta \to \infty$ as follows:

$$f_{ij}(x,y,s,\zeta) = \underbrace{f_{ij\infty}(x,y,s,\zeta)}_{Singular\ Part} + \underbrace{[f_{ij}(x,y,s,\zeta) - f_{ij\infty}(x,y,s,\zeta)]}_{Non\ singular\ Part}, \ i,j \in \{x,y\}. \tag{17}$$

when $\zeta \to \infty$, the asymptotic values of f_{ij} in Eqs. (16) are written as follows:

$$f_{xx\infty}(x,y,s,\zeta)=\frac{2\mu_0 e^{-\zeta y}}{\pi(\kappa+1)}[(2-\zeta y)\cos(\zeta x)b_x(s)+(\zeta y-1)\sin(\zeta x)b_y(s)],$$
$$f_{yy\infty}(x,y,s,\zeta)=\frac{2\mu_0 e^{-\zeta y}}{\pi(\kappa+1)}[\zeta y\cos(\zeta x)b_x(s)-(\zeta y+1)\sin(\zeta x)b_y(s)], \tag{18}$$
$$f_{xy\infty}(x,y,s,\zeta)=\frac{2\mu_0 e^{-\zeta y}}{\pi(\kappa+1)}[(\zeta y-1)\sin(\zeta x)b_x(s)+\zeta y\cos(\zeta x)b_y(s)].$$

The stress components mentioned in Eqs. (15) by view of Eqs. (17) and (18) are as follows:

$$\sigma^*_{xx}(x,y,s)=\frac{2\mu_0}{\pi(\kappa+1)}\frac{y(3x^2+y^2)b_x(s)+x(y^2-x^2)b_y(s)}{(x^2+y^2)^2}+\int_0^\infty[f_{xx}(x,y,s,\zeta)-f_{xx\infty}(x,y,s,\zeta)]d\zeta,$$
$$\sigma^*_{yy}(x,y,s)=\frac{2\mu_0}{\pi(\kappa+1)}\frac{y(y^2-x^2)b_x(s)-x(x^2+3y^2)b_y(s)}{(x^2+y^2)^2}+\int_0^\infty[f_{yy}(x,y,s,\zeta)-f_{yy\infty}(x,y,s,\zeta)]d\zeta, \tag{19}$$
$$\tau^*_{xy}(x,y,s)=\frac{2\mu_0}{\pi(\kappa+1)}\frac{x(y^2-x^2)b_x(s)-y(y^2-x^2)b_y(s)}{(x^2+y^2)^2}+\int_0^\infty[f_{xy}(x,y,s,\zeta)-f_{xy\infty}(x,y,s,\zeta)]d\zeta,$$

The integrals expressed in Eqs. (19) are bounded and can be solved by appropriate numerical methods.

3 SEVERAL INTERFACE CRACKS FORMULATION

To numerical examine an FG half-plane with homogeneous coating containing N interface cracks; the solutions of edge dislocations acquired in the preceding section are utilized. A crack configuration at the interface of the two zones under discussion is defined parametrically as follows:

$$\begin{aligned} &x_i(p)=x_{0i}+pl_i,\\ &y_i(p)=0, \qquad -1\le p\le 1,\ \ i\in\{1,2,3,...,N\}\end{aligned} \tag{20}$$

where $(x_{0i},0)$, l_i illustrate the coordinates of the center and half the length of the *i-th* crack, respectively. Using the principle of superposition of stress field components at a point with (x_i,y_i) coordinates, where the parameter $-1\le p\le 1$, on the faces of all cracks obtains the following relations.

$$\begin{bmatrix}\sigma^*_{yy}(x_i(p),y_i(p),s)\\ \sigma^*_{xy}(x_i(p),y_i(p),s)\end{bmatrix}=\sum_{k=1}^{N}l_k\int_{-1}^{1}[\begin{bmatrix}k^{11}_{yyik}(p,q,s)\\ k^{11}_{xyik}(p,q,s)\end{bmatrix}b_{xk}(q,s)+\begin{bmatrix}k^{12}_{yyik}(p,q,s)\\ k^{12}_{xyik}(p,q,s)\end{bmatrix}b_{yk}(q,s)]dq, i=1,2,...,N, -1\le p\le 1. \tag{21}$$

where $b_{xk}(q,s)$ and $b_{yk}(q,s)$ are the Laplace transforms of the dislocation density functions on the face of *k-th* crack, $k^{1m}_{ik}, m=1,2, i,k=x,y$ are coefficients of $b_x(s)$ and $b_y(s)$ in Eqs. (19). The kernels in Eqs. (21) show the singularity of the Cauchy form for $i=k$ as $q\to p$ and are expressed as follows:

$$k^{1d}_{ryii}(p,q,s)=-\frac{2\mu_0}{\pi l_i(\kappa+1)(p-q)}+\sum_{m=0}^{\infty}a_{1d,mi}(q,s)(p-q)^m \qquad d\in\{1,2\}, r\in\{x,y\} \tag{22}$$

The singular part of the above equation is obtained by expanding the Taylor series $x_i(q)$ and $y_i(q)$ in the vicinity of q. The stresses due to the external load on the presumed crack surfaces between the two materials are to the left-hand side of Eqs. (21), which is placed in the above equations according to the Bueckner's theorem [32] of

superposition with the opposite sign. The integral Eqs. (21) must be solved with the following single-valued conditions:

$$\int_{-1}^{1} b_{kj}(q,s)dq = 0,\ k \in \{x,y\},\ j \in \{1,2,...,N\} \tag{23}$$

The stress components near the crack tip have a square root singularity. So, the density of dislocation is considered as follows:

$$b_{ki}(q,s) = \frac{g_{ki}(q,s)}{\sqrt{1-q^2}},\ k \in \{x,y\},\ -1 < q < 1,\ i \in \{1,2,...,N\} \tag{24}$$

By replacing Eqs. (24) into Eqs. (21) and (23), and using the Lobatto–Chebyshev integration formula, the discretization singular integral equations lead to:

$$\int_{-1}^{1} k^{1h}_{myij}(p,q,s)\frac{g_{ij}(q,s)}{\sqrt{1-q^2}}dq = \frac{\pi}{n-1}\sum_{r=1}^{n} e_r k^{1h}_{myij}(p_d,q_r,s)g_{ij}(q_r,s),\quad m \in \{x,y\},\ h \in \{1,2\} \tag{25}$$

where the collocation points are chosen as $q_r = \cos[\frac{(r-1)\pi}{n-1}],\ r \in \{1,2,...,n\}$, $p_d = \cos[\frac{(2d-1)\pi}{2(n-1)}],\ d \in \{1,2,...,n-1\}$, $e_r = 0.5$ for $r = 1,n$ and $e_r = 1$ for $1 < r < n$. The modes I and II DSIFs are defined by Baghestani et al. [33] as follows:

$$K^*_I(s) = \lim_{r\to 0}\sqrt{2r}\,\sigma^*_{yy}(r,\theta,s),\quad K^*_{II}(s) = \lim_{r\to 0}\sqrt{2r}\,\sigma^*_{xy}(r,\theta,s). \tag{26}$$

where r is the distance from the crack tip, $\theta = 0$ is right and $\theta = \pi$ is left crack tips, respectively. By placing Eqs. (22) and (24) in the Eqs. (21) and use the result in the Eqs. (26), DSIFs are written at the tip of the *i-th* crack in terms of dislocation densities as follows:

$$\begin{aligned} K^*_{Ii}(s) &= -\frac{2\mu_0\eta}{\kappa+1}\sqrt{l_i}\,g_{yi}(\eta,s), \\ K^*_{IIi}(s) &= -\frac{2\mu_0\eta}{\kappa+1}\sqrt{l_i}\,g_{xi}(\eta,s),\ i \in \{1,2,...,N\}. \end{aligned} \tag{27}$$

where $\eta = 1$ is the right crack tip and $\eta = -1$ is the left crack tip. To perform the Laplace inversion, the algorithm developed by Stehfest [31] is used as follows:

$$K_{ji}(t) \approx \frac{l\,n\,2}{t}\sum_{m=1}^{M} H_m K_{jki}(\frac{l\,n\,2}{t}m),\qquad j \in \{I,II\},\ i \in \{1,2,...,N\},\ t > 0 \tag{28}$$

where M is a chosen positive even number, and H_m is given by:

$$H_m = (-1)^{\frac{M}{2}+m}\sum_{n=[0.5(m+1)]}^{\min(\frac{M}{2},m)} \frac{n^{\frac{M}{2}}(2n)!}{(\frac{M}{2}-n)!\,n!\,(n-1)!(m-n)!(2n-m)!} \tag{29}$$

In the above equation [.] signifies the integer part of the quantity.

4 RESULTS AND DISCUSSION

This part of the research is divided into two main sections. At first a numerical example is verified and then the effects of crack characteristics such as crack length, the interaction between of cracks and arrangements of cracks are considered. In order to further investigate the modifiable properties of materials, also the defining and determining properties such as the loading conditions, the variation of time, thickness of the coating and different values of the nonhomogeneous parameter on the DSIFs diagrammatically are shown. In the calculation method, the plane strain conditions with Poisson's ratio $\upsilon = 0.3$, modulus of elasticity $E_0 = 200GPa$, number of Laplace transform inversion points $M = 10$ and mass density $\rho_0 = 7840\,kg/m^3$ are considered. In addition, the DSIFs are normalized by $K_0 = \sigma_0\sqrt{l}$ and $K_0 = \tau_0\sqrt{l}$ for normal and shear traction, respectively, where l is the half length of the crack and K_0 is the static value of SIF for a single crack in a homogenous plane under static traction. In this paper, K_I and K_{II} designate the SIFs for mode I and II of fracture mechanics, respectively.

The first reliability of this study is checked by considering a crack in a homogeneous plane by choosing $\beta = 0$ and $h \to \infty$. A crack with a length $2l = 2cm$ is shown in Fig. 2. The uniform normal step function tractions are applied along the crack face. The variation of the K_I/K_0, versus the t/t_0 are displayed in Fig. 3, where $t_0 = l\sqrt{\rho_0/\mu_0}$. It can be seen from Fig. 3 that a very good agreement has been achieved between the present paper and the results reported by Sih et al. [34] and Mottale et al. [35].

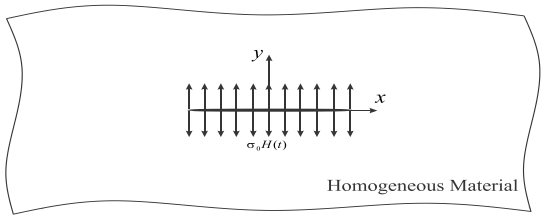

Fig.2
A crack in a homogeneous material under the uniform normal step function traction.

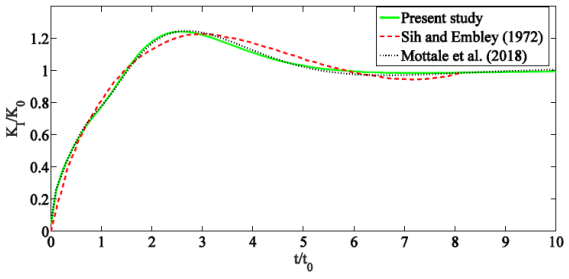

Fig.3
Comparison of dimensionless mode I DSIFs versus t/t_0 for a homogeneous plane.

The second validation of this analysis is investigated by considering a nonhomogeneous elastic half-plane and an elastic half-plane including a crack under normal loading. In this case, we let $h \to \infty$ and $\beta l = 0.5, 1.0$, $2l = 2cm$. The results are easily compared with the solution reported by Jafari et al. [36]. As shown in Fig. 4, excellent matching with Ref [36] is seen.

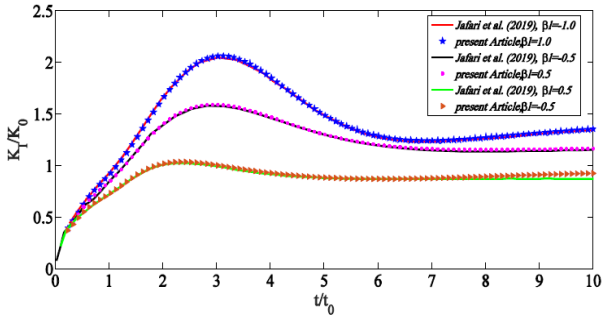

Fig.4
Comparison of dimensionless mode I DSIFs versus t/t_0 for a nonhomogeneous elastic half-plane and an elastic half-plane containing a single crack at the interface.

In Figs.5, 6 and 7, an FG half-plane with a homogeneous coating with $\beta l = 0.25, 0.5$ are considered, including a crack situating at the interface with crack length $2l = 0.2, 0.4cm$ under uniform normal, shear step function traction and mixed mode loading, respectively.

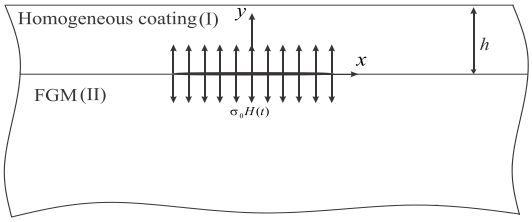

Fig.5
The geometry of a single crack situated between an FG half-plane and homogeneous coating subjected to normal step function traction.

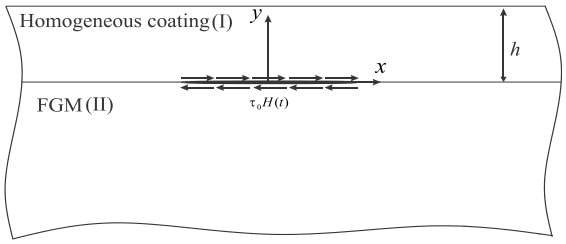

Fig.6
The geometry of a single crack situated between an FG half-plane and homogeneous coating subjected to shear step function traction.

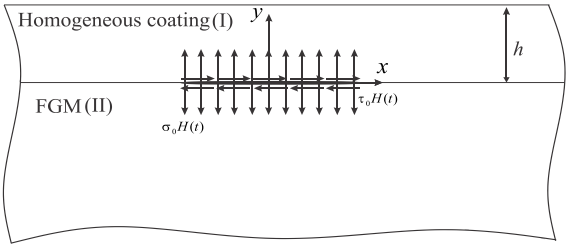

Fig.7
The geometry of a single crack situated between an FG half-plane and homogeneous coating subjected to mixed-mode loading.

The normalized modes I and II transient DSIFs for different dimensionless nonhomogeneous parameters $\beta l = 0.25, 0.5$ are illustrated in Figs. 8 and 9 for normal traction, are shown in Figs. 10 and 11 for shear traction and are plotted in Figs. 12 and 13 for mixed mode loading respectively. The general characteristic of these figures is that the transient DSIF change by the time from their initial zero value to stable values in the end. The DSIFs at the left crack tip are the same as those at the right crack tip in mode I under normal traction and mode II under shear traction (Figs. 8 and 11) while for mode II under normal traction and mode I under shear traction, DSIFs at the left crack tip and right crack tip are differences with a negative sign (Figs. 9 and 10). This is because that the problem is symmetry for mode I and anti-symmetric for mode II under normal loading and also the problem is anti-symmetric for mode I and is symmetric for the mode II under shear loading which this phenomenon has been occurred and reported in Tables 2 and 4 in Ref [37]. By increasing the material gradient parameter βl , the half-plane becomes stiffer than the homogeneous coating, and then both the peak and steady values of the DSIFs at the crack tips increase regularly. Also note that due to the nonhomogeneity of the medium, the DSIFs exhibit mixed mode condition even though the loading is from a single mode. As can be seen, the normalized mode I DSIFs under normal and mixed mode loading and mode II DSIFs under the shear traction increase by increasing the crack length.

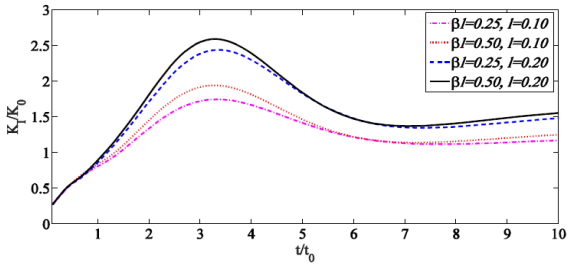

Fig.8
Variations of normalized mode I DSIFs of a single interface crack for different dimensionless nonhomogeneous parameters and crack length under normal traction.

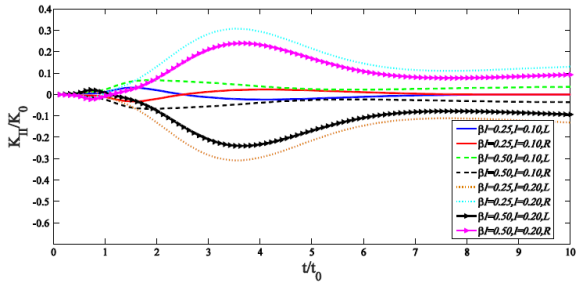

Fig.9
Variations of normalized mode II DSIFs of a single interface crack for different dimensionless nonhomogeneous parameters and crack length under normal traction.

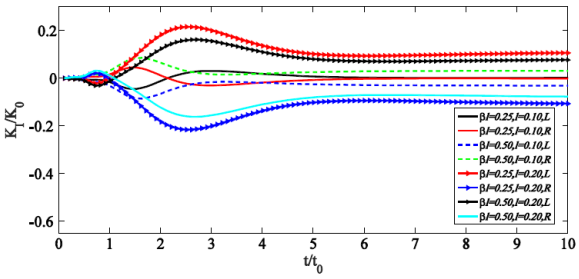

Fig.10
Variations of normalized mode I DSIFs of a single interface crack for different dimensionless nonhomogeneous parameters and crack length under shear traction.

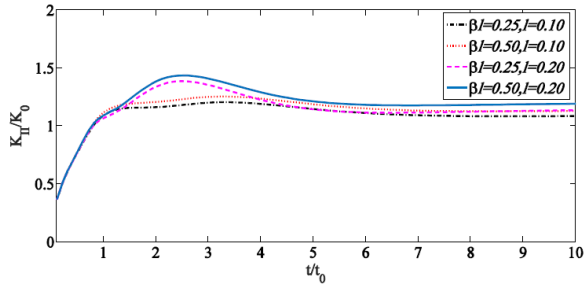

Fig.11
Variations of normalized mode II DSIFs of a single interface crack for different dimensionless nonhomogeneous parameters and crack length under shear traction.

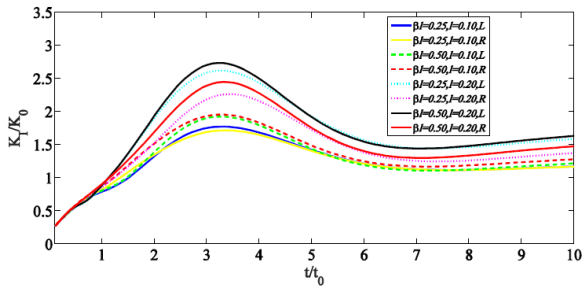

Fig.12
Variations of normalized mode I DSIFs of a single interface crack for different dimensionless nonhomogeneous parameters and crack length under mixed mode loading.

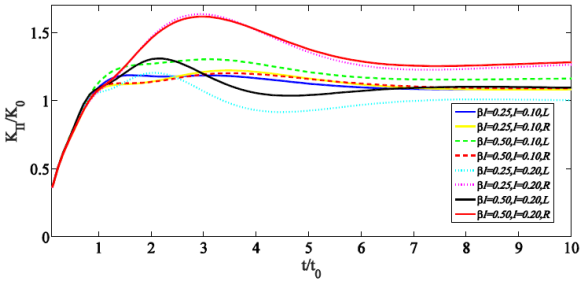

Fig.13
Variations of normalized mode II DSIFs of a single interface crack for different dimensionless nonhomogeneous parameters and crack length under mixed mode loading.

In Figs. 14-19, the variety of normalized modes I and II transient DSIFs with different nonhomogeneous parameters $\beta l = 0.25, 0.5$ and the thickness of the coating $h = 0.1, 0.2$ for an interface crack (Figs. 5-7) are examined. It can be seen that, the thickness of the coating h has only a great effect on the transient DSIFs. Note due

to the lack of symmetry with respect to the *x* axis, the mode I DSIFs are produced under shear traction.

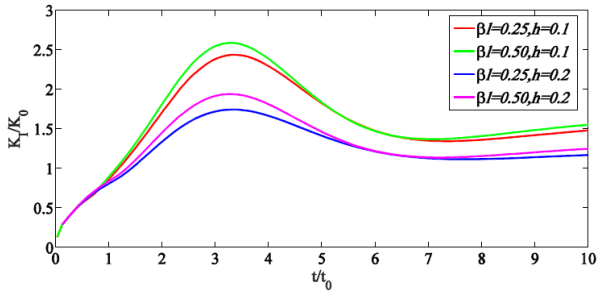

Fig.14
Variations of normalized mode I transient DSIFs of an interface crack for different nonhomogeneous parameters and the thickness of the coating under normal traction.

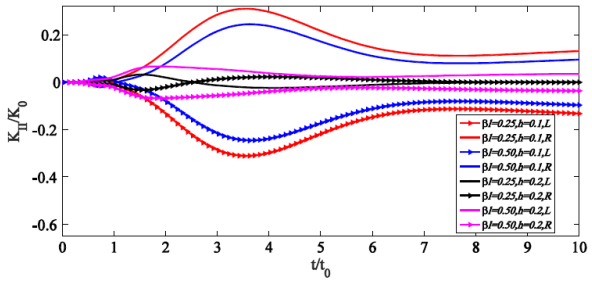

Fig.15
Variations of normalized mode II transient DSIFs of an interface crack for different nonhomogeneous parameters and the thickness of the coating under normal traction.

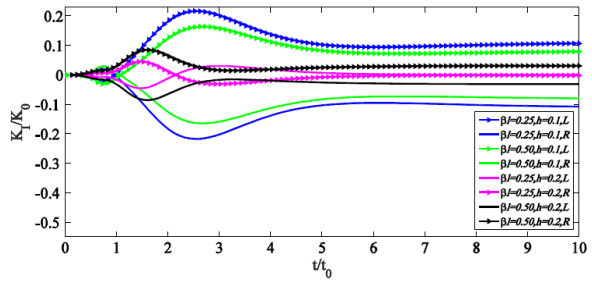

Fig.16
Variations of normalized mode I transient DSIFs of an interface crack for different nonhomogeneous parameters and the thickness of the coating under shear traction.

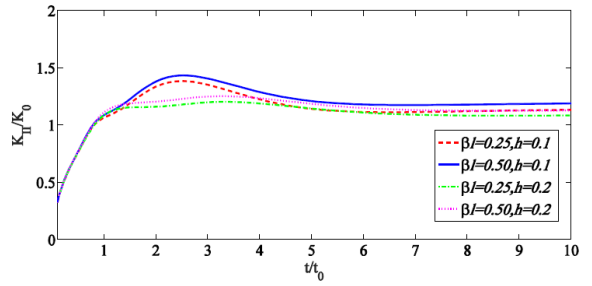

Fig.17
Variations of normalized mode II transient DSIFs of an interface crack for different nonhomogeneous parameters and the thickness of the coating under shear traction.

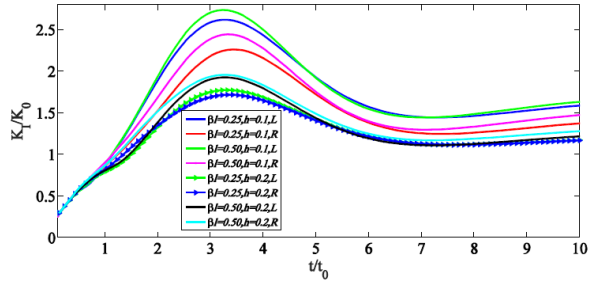

Fig.18
Variations of normalized mode I transient DSIFs of an interface crack for different nonhomogeneous parameters and the thickness of the coating under mixed mode loading.

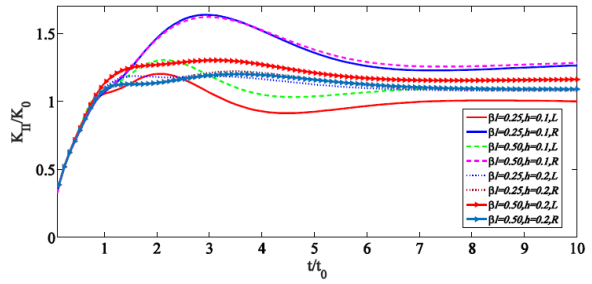

Fig.19
Variations of normalized mode II transient DSIFs of an interface crack for different nonhomogeneous parameters and the thickness of the coating under mixed mode loading.

In Figs. 20-25, the variety of normalized modes I and II transient DSIFs with different the thickness of the coating $h=0.1,0.2$ and the Poisson's ratio $\upsilon=0.3,0.4$, for an interface crack (Figs. 5-7) with nonhomogeneous parameter $\beta l=0.5$ are examined. It can be seen that, the thickness of the coating and the Poisson's ratio has only a great effect on the transient DSIFs.

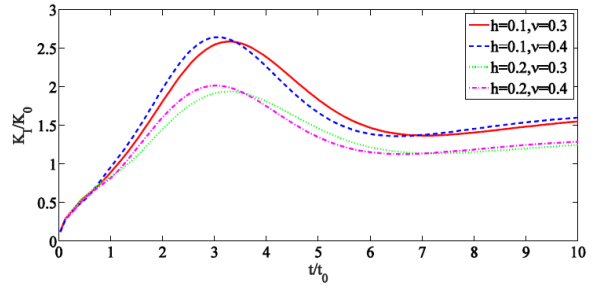

Fig.20
Variations of normalized mode I transient DSIFs of an interface crack for different Poisson's ratio and the thickness of the coating under normal loading.

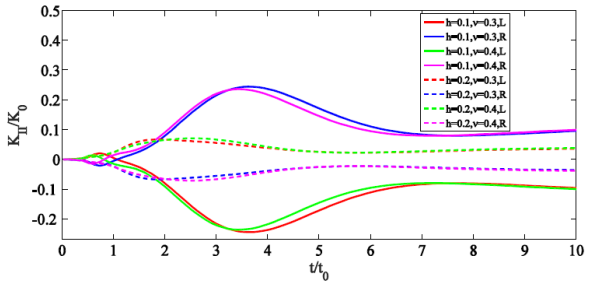

Fig.21
Variations of normalized mode II transient DSIFs of an interface crack for different Poisson's ratio and the thickness of the coating under normal loading.

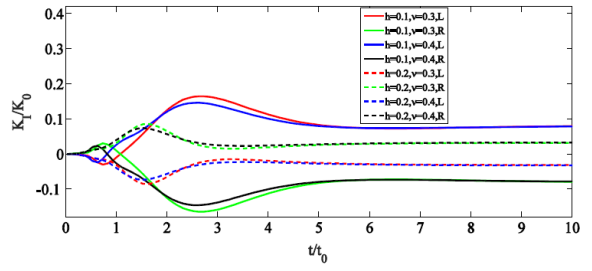

Fig.22
Variations of normalized mode I transient DSIFs of an interface crack for different Poisson's ratio and the thickness of the coating under shear loading.

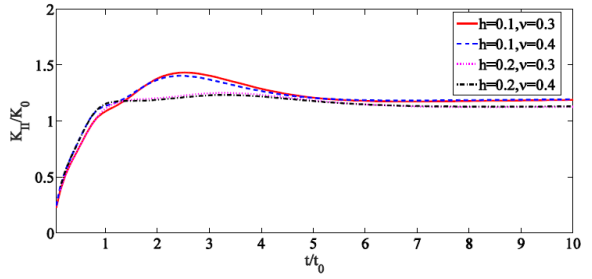

Fig.23
Variations of normalized mode II transient DSIFs of an interface crack for different Poisson's ratio and the thickness of the coating under shear loading.

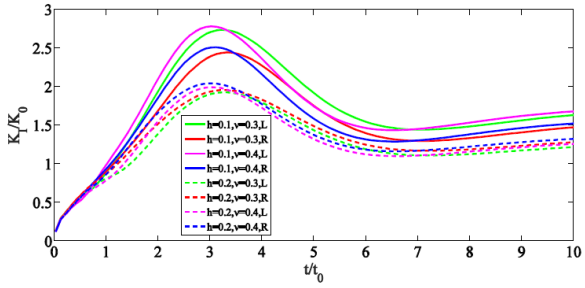

Fig.24
Variations of normalized mode I transient DSIFs of an interface crack for different Poisson's ratio and the thickness of the coating under mixed mode loading.

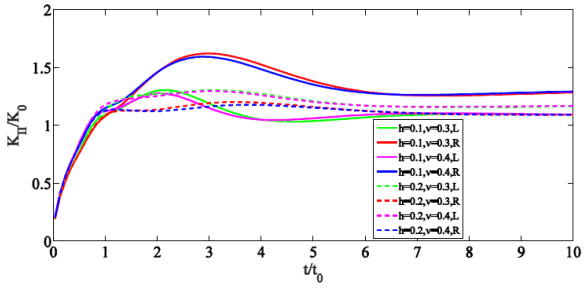

Fig.25
Variations of normalized mode II transient DSIFs of an interface crack for different Poisson's ratio and the thickness of the coating under mixed mode loading.

The geometry of two cracks at the interface between an FG half-plane and homogeneous coating, under uniform normal and shear load is displayed in Figs. 26 and 27. For mode I and II DSIFs, the interaction between two cracks with two dimensionless nonhomogeneous parameters $\beta l = 0.5, 1.0$ under normal loading are depicted in Figs. 28 and 29, respectively, where $h/l = 2.0$ and dimensionless distant $x_{c1}/l = x_{c2}/l = 1.2$. Due to the symmetry of the problem with respect to the *y*-axis, DSIFs in mode I at the tips L_1, R_1 are equal to those at R_2, L_2, respectively. The variations of DSIFs at tips L_1, R_2 are much higher than that at the tips R_1, L_2, because these tips have stronger interaction than tips R_1, L_2. Also, it can be observed that, the magnitudes of DSIFs for mode I increase with the increasing of the nonhomogeneous parameter.

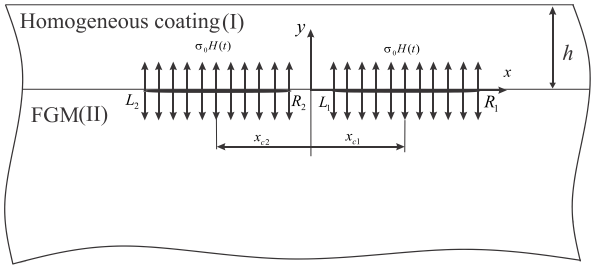

Fig.26
The geometry of two cracks situated between an FG half-plane and homogeneous coating subjected to normal loading.

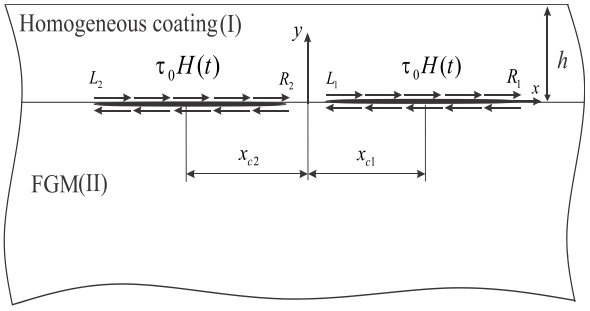

Fig.27
The geometry of two cracks situated between an FG half-plane and homogeneous coating subjected to shear loading.

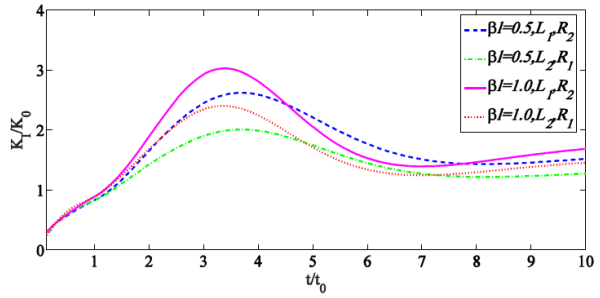

Fig.28
Interaction of mode I of two interface cracks under normal step function traction**.**

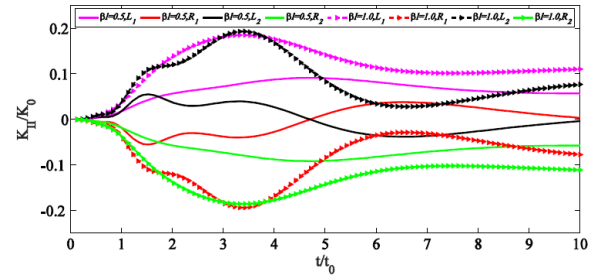

Fig.29
Interaction of mode II of two interfaces cracks under normal step function traction.

Similar to the two previous examples, in Figs. 30 and 31 the variations of normalized DSIFs versus t/t_0 for different values of $\beta l = 0.5,1.0$ under shear loading are considered. The thickness of the coating and center of cracks are taken to be $h/l = 2.0$ and $x_{c1}/l = x_{c2}/l = 1.2$, respectively. Obviously, the maximum DSIFs for the crack tips occur when the crack length is increased. In addition, by increasing the crack length the distance between two cracks decreased and due to the interaction of two cracks the DSIFs of the crack tips are increased.

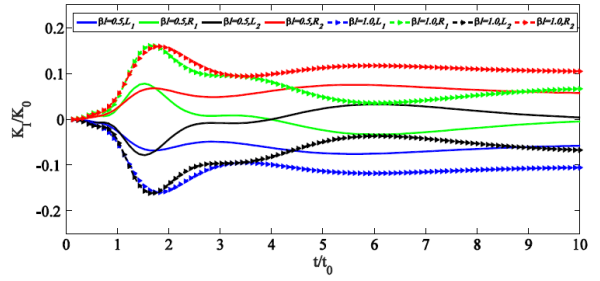

Fig.30
Interaction of mode I of two interfaces cracks under shear loading for different values βl.

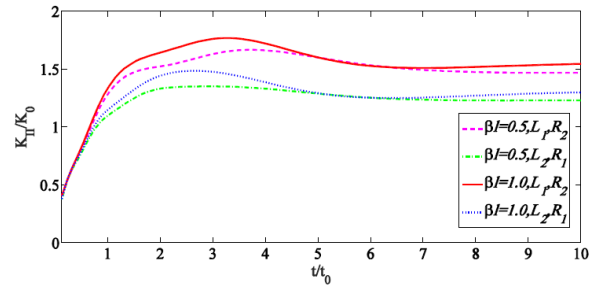

Fig.31
Interaction of mode II of two interfaces cracks under shear loading for different values βl.

In Fig. 32 the geometry of three equal cracks with lengths $2l = 2cm$ located at the interface of an FG half-plane and homogeneous coating with identical center-to-center distance $x_{c2}/l = x_{c3}/l = 2.1$ under normal loading is displayed. The variation of normalized modes I and II transient DSIFs versus the dimensionless time for nonhomogeneous parameter $\beta l = 0.5$ are plotted in Figs. 33 and 34, respectively. As the problem is symmetrical, the values of the mode I DSIFs at the tips L_1R_1, L_3R_2 and L_2R_3 are identical. It is found from Figs. 33 and 34 the

mode I DSIFs at the tips of crack L_1R_1 is higher than that the other tips.

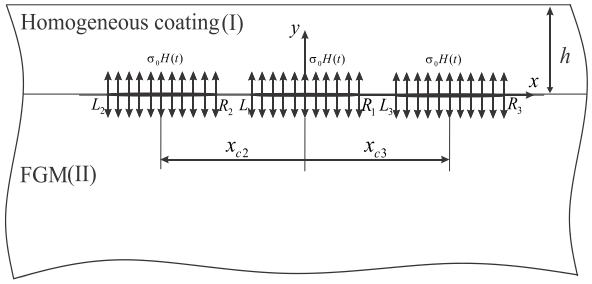

Fig.32
The geometry of three cracks located between an FG half-plane and homogeneous coating subjected to uniform normal step function.

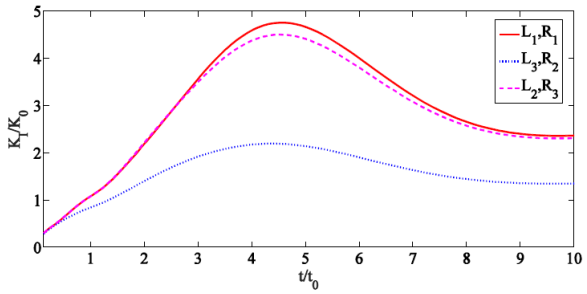

Fig.33
Interaction of mode I of three interface cracks under normal step function traction.

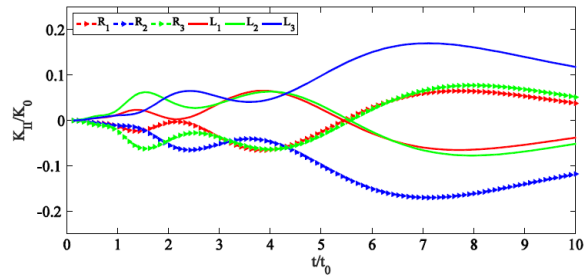

Fig.34
Interaction of mode II of three interface cracks under normal step function traction.

5 CONCLUSIONS

An FG half-plane with homogeneous coating weakened by multiple interface cracks are studied under mixed mode impact loading. In this paper, the FG material properties are supposed to change continuously along the *y*-axis in the nonhomogeneous half-planes, and the crack faces are loaded by uniform normal, shear step function traction and mixed mode loading. Using the DDT and integral transform methods, the associated boundary value problem is reduced to singular integral equations for the Volterra type climb and glide edge dislocation density. Validation of the presented method is carried out by considering a single crack in an isotropic infinite plane and also a nonhomogeneous elastic half-plane and an elastic half-plane under normal impact loading. The numerical results of the multiple interface cracks revealed that:

(1) The nonhomogeneous parameters significantly effect on the transient DSIFs while the Poisson ratio has only a negligible influence on the transient DSIFs.
(2) The values of DSIFs for two and three cracks are larger than for the single crack because of the interaction between cracks tips in several cracks are greater than that of the single crack tip.
(3) The results are compatible with the analytical solutions obtained in Sih and Embley [34], Mottale et al. [35] and Jafari et al. [36].
(4) The maximum DSIFs for the crack tips occur when the crack length is increased.
(5) By increasing the crack length the distance between two cracks decreased and due to interaction of two cracks the DSIFs of the crack tips are increased.

APPENDIX I

Parameters appearing in Eq. (14) are:

$$A_{31}=\Big\{[(\sinh(hr_1)\sinh(hr_2)b_{14}^2b_{23}^2-2(-1+\cosh(hr_1)\cosh(hr_2))b_{13}b_{14}b_{23}b_{24}+(\sinh(hr_1)\sinh(hr_2)b_{13}^2b_{24}^2)a_{41}]$$
$$+[(-\sinh(hr_1)\sinh(hr_2)b_{11}b_{14}b_{23}^2-\sinh(hr_1)\sinh(hr_2)b_{21}b_{24}b_{13}^2+(-1+\cosh(hr_1)\cosh(hr_2))$$
$$b_{13}b_{23}(b_{14}b_{21}+b_{11}b_{24}))a_{44}]+[(b_{14}b_{21}-b_{11}b_{24})(\cosh(hr_2)\sinh(hr_1)b_{14}b_{23}-\cosh(hr_1)\sinh(hr_2)b_{13}b_{24})a_{43}]\Big\}/\Delta$$

$$A_{32}=\Big\{[\sinh(hr_1)\sinh(hr_2)b_{14}^2b_{23}^2-2(-1+\cosh(hr_1)\cosh(hr_2))b_{13}b_{14}b_{23}b_{24}+(\sinh(hr_1)\sinh(hr_2)b_{13}^2b_{24}^2]$$
$$+[(b_{13}-b_{23})(-\cosh(hr_1)\sinh(hr_2)b_{23}b_{14}-\cosh(hr_2)\sinh(hr_1)b_{13}b_{24})a_{44}]$$
$$+[(\sinh(hr_1)\sinh(hr_2)b_{14}^2b_{23}-(-1+\cosh(hr_1)\cosh(hr_2))b_{14}(b_{13}+b_{23})b_{24}+\sinh(hr_1)\sinh(hr_2)b_{13}b_{24}^2)a_{43}]\Big\}/\Delta$$

$$A_{41}=\Big\{-[(\sinh(hr_1)\sinh(hr_2)b_{14}^2b_{23}^2-2(-1+\cosh(hr_1)\cosh(hr_2))b_{13}b_{14}b_{23}b_{24}+(\sinh(hr_1)\sinh(hr_2)b_{13}^2b_{24}^2)a_{31}]$$
$$+[(-\sinh(hr_1)\sinh(hr_2)b_{11}b_{14}b_{23}^2-\sinh(hr_1)\sinh(hr_2)b_{21}b_{24}b_{13}^2+(-1+\cosh(hr_1)\cosh(hr_2))$$
$$b_{13}b_{23}(b_{14}b_{21}+b_{11}b_{24}))a_{34}]-[(b_{14}b_{21}-b_{11}b_{24})(\cosh(hr_2)\sinh(hr_1)b_{14}b_{23}-\cosh(hr_1)\sinh(hr_2)b_{13}b_{24})a_{33}]\Big\}/\Delta$$

$$A_{42}=\Big\{-[\sinh(hr_1)\sinh(hr_2)b_{14}^2b_{23}^2-2(-1+\cosh(hr_1)\cosh(hr_2))b_{13}b_{14}b_{23}b_{24}+(\sinh(hr_1)\sinh(hr_2)b_{13}^2b_{24}^2]$$
$$+[(b_{13}-b_{23})(\cosh(hr_1)\sinh(hr_2)b_{23}b_{14}-\cosh(hr_2)\sinh(hr_1)b_{13}b_{24})a_{34}]$$
$$+[(\sinh(hr_1)\sinh(hr_2)b_{14}^2b_{23}-(-1+\cosh(hr_1)\cosh(hr_2))b_{14}(b_{13}+b_{23})b_{24}+\sinh(hr_1)\sinh(hr_2)b_{13}b_{24}^2)a_{33}]\Big\}/\Delta$$

$$\Delta=(b_{13}b_{14}b_{21}+b_{11}b_{24}b_{23})(a_{34}a_{43}-a_{33}a_{44})+b_{13}b_{23}(b_{14}b_{21}+b_{11}b_{24})(a_{44}-a_{34})+(b_{13}b_{14}b_{24}+b_{14}b_{23}b_{24})$$
$$\times(a_{33}a_{41}-a_{31}a_{43})+2b_{13}b_{14}b_{23}b_{24}(a_{31}-a_{41})+\sinh(hr_2)\{b_{14}b_{23}[\cosh(hr_1)(a_{34}a_{41}-a_{31}a_{44})(b_{13}-b_{23})$$
$$+\sinh(hr_1)((b_{23}-a_{33})(a_{44}b_{11}-a_{41}b_{14})+(a_{34}b_{11}-a_{31}b_{14})(a_{43}-b_{23}))]+b_{13}b_{24}[\cosh(hr_1)(b_{11}b_{24}-b_{14}b_{21})$$
$$\times(a_{33}-a_{43})+\sinh(hr_1)((a_{43}-b_{13})(a_{34}b_{21}-a_{31}b_{24})+(a_{41}b_{24}-a_{44}b_{21})(a_{33}-b_{13}))]\}+\cosh(hr_2)\{\cosh(hr_1)$$
$$\times[b_{14}b_{21}b_{23}(a_{44}(a_{33}-b_{13})+a_{34}(-a_{43}+b_{13}))+b_{13}b_{24}(a_{43}(a_{31}b_{14}-a_{34}b_{11})+a_{33}(a_{44}b_{11}-a_{41}b_{14}))$$
$$+b_{23}b_{24}(b_{11}b_{13}(a_{34}-a_{44})-a_{41}b_{14}(a_{33}-2b_{13})+a_{31}b_{14}(a_{43}-2b_{13}))]+\sinh(hr_1)[b_{13}b_{24}(b_{23}-b_{13})(a_{34}a_{41}-a_{31}a_{44})$$
$$+b_{23}b_{14}(a_{33}-a_{43})(b_{14}b_{21}-b_{11}b_{24})]\}$$

REFERENCES

[1] Ma L., Wu L.Z., Guo L.C., 2002, Dynamic behavior of two collinear anti-plane shear cracks in a functionally graded layer bonded to dissimilar half planes, *Mechanics Research Communications* **29**: 207-215.

[2] El-Borgi S., Erdogan F., Ben Hatira F., 2003, Stress intensity factors for an interface crack between a functionally graded coating and a homogeneous substrate, *International Journal of Fracture* **123**: 139-162.

[3] Chi S., Chung Y.L., 2003, Cracking in coating–substrate composites with multi-layered and FGM coatings, *Engineering Fracture Mechanics* **70**: 1227-1243.

[4] Huang G.Y., Wang Y.S., Gross D., 2003, Fracture analysis of functionally graded coatings: plane deformation, *European Journal of Mechanics; A/Solids* **22**: 535-544.

[5] Ma L., Wu L.Z., Zhou Z.G., 2004, Dynamic stress intensity factors around two parallel cracks in a functionally graded layer bonded to dissimilar half-planes subjected to anti-plane incident harmonic stress waves, *International Journal of Engineering Science* **42**: 187-202.

[6] Dag S., Yildirim B., Erdogan F., 2004, Interface crack problems in gradedorthotropic media: Analytical and computational approaches, *International Journal of Fracture* **130**: 471-496.

[7] Liu L., Kardomateas G.A., Holmes J.W., 2004, Mixed-mode stress intensity factors for a crack in an anisotropic bi-material strip, *International Journal of Solids and Structures* **41**: 3095-3107.

[8] Guo L.C., Wu L.Z., Zeng T., Cao D., 2005, The transient response of a coating–substrate structure with a crack in the functionally graded interfacial layer, *Composite Structures* **70**: 109-119.

[9] Li X.F., 2005, Two perfectly-bonded dissimilar orthotropic strips with an interfacial crack normal to the boundaries, *Applied Mathematics and Computation* **163**: 961-975.

[10] Huang G.Y., Wang Y.S., Yu S.W., 2005, A new model for fracture analysis of functionally graded coatings under plane deformation, *Mechanics of Materials* **37**: 507-516.

[11] Chen J., 2005, Determination of thermal stress intensity factors for an interface crack in a graded orthotropic coating-substrate structure, *International Journal of Fracture* **133**: 303-328.

[12] Long X., Delale F., 2005, The mixed mode crack problem in an FGM layer bonded to a homogeneous half-plane, *International Journal of Solids and Structures* **42**: 3897-3917.
[13] Yong dong L., Bin J., Nan Z., Li qiang T., Yao D., 2006, Dynamic stress intensity factor of the weak/micro-discontinuous interface crack of a FGM coating, *International Journal of Solids and Structures* **43**: 4795-4809.
[14] Ioka S., Masuda K., Kubo S., 2007, Singular stress field near the edge of interface of bonded dissimilar materials with an interlayer, *International Journal of Solids and Structures* **44**: 6232-6238.
[15] Li X.F., Fan T.Y., 2007, Dynamic analysis of a crack in a functionally graded material sandwiched between two elastic layers under anti-plane loading, *Composite Structures* **79**: 211-219.
[16] Guo L.C., Noda N., 2008, Dynamic investigation of a functionally graded layered tructure with a crack crossing the interface, *International Journal of Solids and Structures* **45**: 336-357.
[17] Li Y.D., Lee K.Y., 2009, Anti-plane fracture analysis for the weak-discontinuous interface in a non-homogeneous piezoelectric bi-material structure, *European Journal of Mechanics; A/Solids* **28**: 241-247.
[18] Peng X.L., Li X.F., 2009, Transient response of the crack-tip field in a magnetoelectroelastic half-space with a functionally graded coating under impacts, *Archive of Applied Mechanics* **79**: 1099-1113.
[19] Torshizian M.R., Kargarnovin M.H., 2010, Anti-plane shear of an arbitrary oriented crack in a functionally graded strip bonded with two dissimilar half-planes, *Theoretical and Applied Fracture Mechanics* **54**: 180-188.
[20] Cheng Z., Gao D., Zhong Z., 2010, Crack propagating in functionally graded coating with arbitrarily distributed material properties bonded to homogeneous substrate, *Acta Mechanica Solida Sinica* **23**: 437-446.
[21] Cheng Z., Gao D., Zhong Z., 2012, A moving interface crack between two dissimilar functionally graded strips under plane deformation with integral equation methods, *Engineering Analysis with Boundary Elements* **36**: 267-273.
[22] Shi P.P., 2015, Interaction between the doubly periodic interfacial cracks in a layered periodic composite: Simulation by the method of singular integral equation, *Theoretical and Applied Fracture Mechanics* **78**: 25-39.
[23] Fallahnejad M., Bagheri R., Noroozi M., 2018, Transient analysis of two dissimilar FGM layers with multiple interface cracks, *Structural Engineering and Mechanics* **67**: 277-281.
[24] Bagheri R., 2019, Transient behavior of multiple interface cracks in two non-homogeneous half-layers, *Iranian Journal of Science and Technology Transactions of Mechanical Engineering* **44**: 619-629.
[25] Bagheri R., Monfared M.M., 2020, In-plane transient analysis of two dissimilar nonhomogeneous half-planes containing several interface cracks, *Acta Mechanica* **231**: 3779-3797.
[26] Bagheri R., Monfared M.M., 2021, Mixed-mode fracture analysis for two dissimilar half-planes with multiple interface moving cracks, *Wave Random Complex* **31**: 1-23.
[27] Bagheri R., Enjilela V., 2021, Time-harmonic analysis of multiple interface cracks in two dissimilar FGM half-planes: In-plane problem, *Theoretical and Applied Fracture Mechanics* **116**: 103094.
[28] Bagherpoor F., Pourseifi M., 2022, Dynamic mode III stress intensity factors of multiple axisymmetric interfacial cracks in an FGM coated orthotropic layer, *International Journal for Computational Methods in Engineering Science and Mechanics* **2**:1-7.
[29] Rabieifar A., Pourseifi M., Derili H. 2018, Transient analysis for torsional impact of multiple axisymmetric cracks in the functionally graded orthotropic medium, *The IMA Journal of Applied Mathematics* **83**: 131-47.
[30] Monfared M.M., Pourseifi M., Bagheri R., 2019, Computation of mixed mode stress intensity factors for multiple axisymmetric cracks in an FGM medium under transient loading, *International Journal of Solids and Structures* **58**: 220-231.
[31] Stehfest H., 1970, Algorithm 368: Numerical inversion of Laplace transforms [D5], *Communications of the ACM* **13**: 47-49.
[32] Bueckner H., 1958, The propagation of cracks and the energy of elastic deformation, *Transaction of the ASME Series E* **80**: 1225-1230.
[33] Baghestani A.M., Fotuhi A.R., Fariborz S.J., 2013, Multiple interacting cracks in an orthotropic layer, *Archive of Applied Mechanics* **83**: 1549-1567.
[34] Sih G., Embley G., Ravera R., 1972, Impact response of a finite crack in plane extension, *International Journal of Solids and Structures* **8**: 977-993.
[35] Mottale H., Monfared M.M., Bagheri R., 2018, The multiple parallel cracks in an orthotropic non-homogeneous infinite plane subjected to transient in-plane loading, *Engineering Fracture Mechanics* **199**: 220-234.
[36] Jafari A., Monfared M.M., Bagheri R., 2019, Mixed‐mode computation of the transient dynamic stress intensity factor for multiple interface cracks, *Journal of the Brazilian Society of Mechanical Sciences* **41**: 573.
[37] Monfared M.M., Ayatollahi M., 2016, Multiple crack problems in nonhomogeneous orthotropic planes under mixed mode loading conditions, *Engineering Fracture Mechanics* **155**: 1-17.